Glass cutting by femtosecond pulsed irradiation

Egidijus Vanagas
Jouji Kawai
Dmitrii Tuzhilin
Igor Kudryashov
Tokyo Instruments Inc.
6-18-14 Nishikasai
Edogawa-ku, Tokyo 134-0088, Japan

Atsushi Mizuyama
Kazutaka G. Nakamura
Ken-Ichi Kondo
Tokyo Institute of Technology
Materials and Structures Laboratory
4259 Nagatsuta-cho
Midori-ku, Yokohama-shi
Kanagawa 226-8503, Japan

Shin-ya Koshihara
Masaki Takesada
Kazunari Matsuda
Kanagawa Academy of Science
and Technology
KSP East 301
3-2-1 Sakado Takatsu-ku
Kawasaki-shi Kanagawa 213-0012, Japan

Saulius Juodkazis*
Vygandas Jarutis
Shigeki Matsuo
CREST-JST
The University of Tokushima
2-1 Minamijosanjima
Tokushima 770-8506, Japan
E-mail: saulius@eco.tokushima-u.ac.jp

Hiroaki Misawa
CREST-JST
Hokkaido University
Research Institute for Electronic Science
Sapporo 060-0812, Japan
E-mail address: misawa@es.hskudai.ac.jp

Abstract. We report on quartz and glass cutting by a lateral scanning of femtosecond pulses (150 fs at 1 kHz repetition rate) of 800 nm wavelength at room and low pressure (5 Torr) air ambience. Pulses were focused by a low numerical aperture (NA$\leqslant$0.1) objective lens. Optimization of fabrication conditions: pulse energy and scanning speed were carried out to achieve large-scale (millimeter-to-centimeter) cutting free of microcracks of submicron dimensions along the edges and walls of the cut. Cutting through out the samples of 0.1–0.5 mm thickness was successfully achieved without apparent heat affected zone. At low air pressure (5 Torr) ambience, redeposition of ablated material was considerably reduced. It is demonstrated that the damage on the rear surface was induced by the stress waves, which originated from the plasma ablation pressure pulse. The mechanism of femtosecond-laser cutting of transparent materials at high irradiance and the influence of stress waves generated by plasma plume are discussed. [DOI: 10.1117/1.1668274]

Subject terms: femtosecond laser microfabrication, ablation, glass and quartz dicing

Paper JM3 02021 received Jun. 4, 2002; revised manuscript received Aug. 29, 2003; accepted for publication Sep. 2, 2003.

1 Introduction

Femtosecond (fs) laser microfabrication is capable of recording waveguides,[1,2] three-dimensional (3-D) optical memory,[3,4] photonic crystal structures[5] in glasses and polymers.[6,7] In conjunction with wet etching, micro channels can be developed in glass preliminary exposed to fs pulses.[8,9] A 3-D submicron structuring of transparent materials is a distinctive field of application for ultra-short pulses.[10,11] A high intensity allows to achieve 3-D microstructuring at the wavelength in the transmission window of material, e.g., for silicate glasses blue edge of strong absorption ($\alpha > 10^4$ cm^{-1}, here α is the decadic coefficient of absorption) starts at 250 nm and infrared absorption has similar value at 10 μm. However, in the field of large scale (millimeter-to-centimeter) laser dicing, drilling, and cutting fs-lasers are not considered practical as compared with industrial solid state and CO_2 continuous wave/nanosecond (ns)-/picosecond (ps)-lasers. Current trend of miniaturization is constantly increasing requirements for high precision and debris-free processing of complex multicomponent micro-electro-mechanical system devices, especially, when movable parts are present. Dicing of sapphire or SiC wafers used in GaN-based light emitting and laser diodes industry is another example where current technologies based on long (ps–ns) pulsed lasers cannot provide a viable solution for wafers thinner than 0.1 mm. Also, a heat affected zone (HAZ) should be minimized as much as possible for dicing and cutting wafers with densely packed microchips. In these particular fields application of fs-laser is prospective.

*Present address: Hokkaido University, Research Institute for Electronic Sciences, Sapporo 060-0812, Japan.

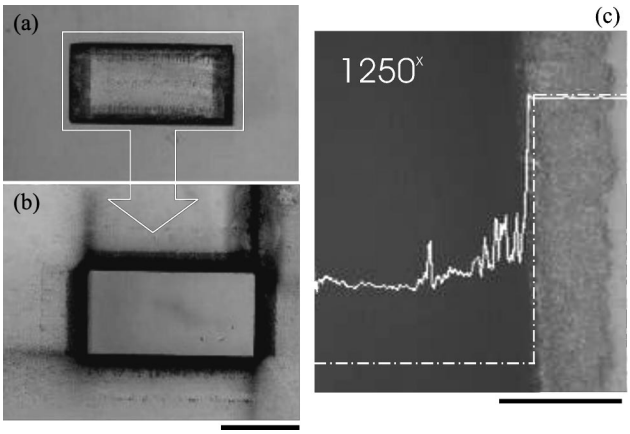

Fig. 1 Optical image of a free-laying square workpiece (a) cut out of quartz plate (b). Pulse duration was 150 fs, wavelength 800 nm, and pulse energy 700 μJ. Cutting was carried out by clockwise scan of the beam at 200 μm/s stage velocity. (c) Edge profile of the groove measured by scanning microscopy. Fabrication conditions: 200 μm/s scanning speed, 400 μJ pulse energy. Thickness of sample is shown by dashed profile. Scale bars, 1 mm (a), (b) and 50 μm (c).

Here, we demonstrate cutting of a sub-millimeter-thick crystalline quartz and glass plates by a train of fs pulses at 800 nm wavelength. Implementation of a low air pressure ambience (5 Torr) allowed significantly reduce redeposition and debris around the processing line and to increase the volumetric ablation rate.

2 Experiment

Laser setup of fs-fabrication was based on oscillator (Mai Tai) with regenerative amplifier both build in one body (Hurricane, both from Spectra Physics) and a micromachining system (Tokyo Instruments, Inc.). Electronic shutter allows switching fs-shooting on and off at a preprogrammed location according to the movement of step-motor stage (Sigma-Koki). The pulse energy was controlled by attenuators built in the micromachining system. Cutting was carried out at pulse intensities well above the dielectric breakdown threshold. A self-made low-pressure vacuum chamber was employed for fabrication at 5 Torr using rotatory pump. In air, the laser irradiation was focused by a plano-convex lens of the focal length of $f=125$ mm; the corresponding f-number was $f/\#=F/D=1/(2\mathrm{NA})\simeq 20.8$, where NA is the numeric aperture, F is the focal length,

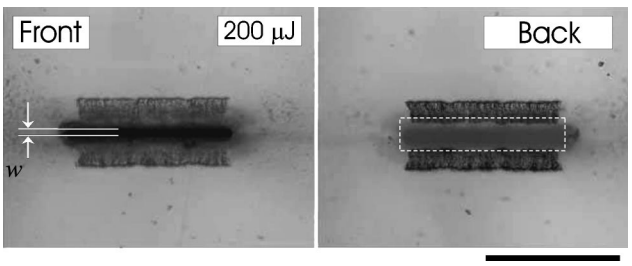

Fig. 2 Optical images of front and rear surfaces of quartz sample cut by fs-irradiation at 200 μJ/pulse energy at 200 μm/s scan speed. Scanning time was 100 s. The width of an ablated groove was $w=120$ μm for 200 μJ (e.g., 150 μm at 700 μJ). Dashed-boxed region marks a rear surface damage. Scale bar, 1 mm.

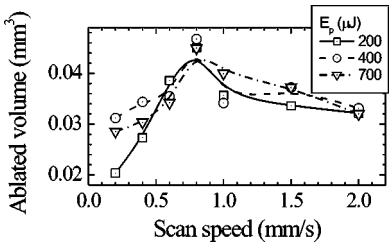

Fig. 3 Ablated volume after a 100 s scan over a 1-mm-long line versus scanning speed for few pulse energies, E_p. Lines are drawn to guide the eye.

and D is the filled aperture of the lens.[12] Then, diffraction limited focusing of a Gaussian beam would correspond to a $2w_0=(f/\#)\cdot 4\lambda/\pi\simeq 21$ μm diameter spot (waist diameter) with the waist length given by doubled Rayleigh length[12] $2z_R=2n\pi\lambda(f/\#)^2\simeq 2.2$ mm (the refractive index $n=1$ for focusing in air). For cutting in vacuum a higher NA lens was used: $2w_0=8.64$ μm and $2z_R=158$ μm. In all experiments laser pulses were focused on the surface and scanned laterally, while the axial position of focus was kept fixed. Polarization at the focus was set circular.

As samples we used crystalline z-cut quartz (α-SiO_2 crystal) and borosilicate cover glass (Matsunami). Thicknesses of quartz and glass samples were 0.30 ± 0.04 mm and 0.15 ± 0.03 mm, respectively. A cut quality was assessed using an optical confocal profiler (Keyence VF-7500) and scanning electron microscope (SEM). For SEM observation samples were coated by 5 nm of Pt.

3 Results

3.1 *Cutting in Air*

Figure 1 shows an example of carving-out workpiece from the sample of crystalline quartz. Laser focus was placed on the front surface of the sample. Since the length of the waist at focus in air was about 2 mm, all fabrication was done in the near-field region of the laser beam without axial change of the focus position. The quartz plate was set and kept at the exact focus with 10 μm tolerance using a confocal system which tracks the surface by reflection of the auxiliary HeNe-laser beam (see for details Ref. 13). The pulse energy for cutting was set 5–10 times larger than the ablation threshold. Dielectric breakdown was first observed on the front/entrance surface, and then it was self-propagating into the bulk of sample. Typical spark emission was observed from the ablation plume. The quality of a laser cut was assessed by the edge sharpness of the ablated groove into a quartz surface as shown in Fig. 1(c). The smoothness of the cut plane defined as a mean min-max roughness was smaller than 2 μm.

Typical optical images of the front and rear surfaces after a 1-mm-long scan for a fixed total time of 100 s are shown in Fig. 2. Gray regions around the ablated channel of width, w, are due to the free-laying ablation products and a secondary damage of the rear surface. The free-laying debris were washable by dipping into a 0.01% water solution of hydrofluoric (HF) acid, while the damage of the rear surface was inevitable consequence of fabrication (discussion follows in Sec. 4.2). Figure 3 summarizes experimen-

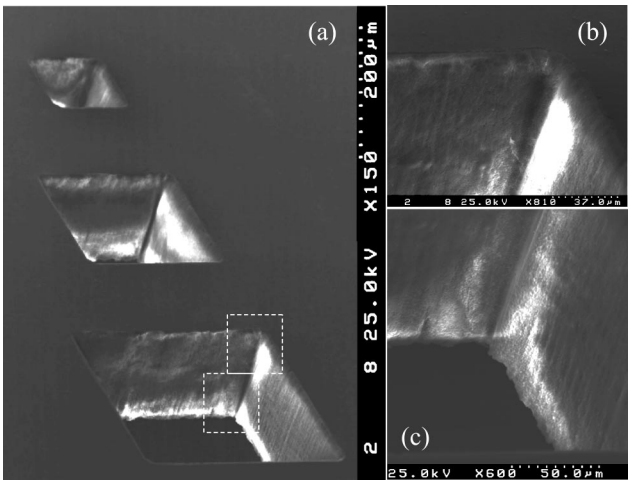

Fig. 4 (a)–(c) SEM images of a cut through cover glass made in low pressure chamber (5 Torr) by 150 fs pulses at 800 nm wavelength. (b), (c) A close-up view of regions marked in (a). Cut was accomplished by 8 scans at 0.5 mm/s scanning speed with 50 μJ energy per pulse at 1 kHz repetition rate.

tal results of ablation rate versus scan velocity, where an ablated volume was calculated from the known width, depth and length of the ablated line. End points (about 0.1-mm-long) of the line were not taken into account for calculations of volume, since the exposure conditions at those particular locations differed from the rest of data due to the reverse in a stage movement. As one can see, there exists an optimum scanning speed for the fastest cut formation. We have further examined the possibility to increase the ablation speed and quality of a cut by carrying the same experiment at low air pressure (Sec. 3.2).

3.2 *Cutting in Vacuum*

In order to achieve debris free fabrication and to increase ablation rate, we have carried out the same cutting experiment in vacuum on glass samples. The effect of low air pressure environment (78% of which is nitrogen) is to increase the mean free path of the gas molecules, thus reducing the probability of chemical reactions and collisions with material being removed from the ablation pit. The mean free path of ideal gas molecules is $l=(N/V)\sqrt{2}\pi z^{2\,-1}$, where N/V and z is the density and effective diameter of the molecules, respectively. It can be roughly estimated, that for N_2 molecules in air $l\simeq 76$ nm at normal conditions, and $l\simeq 11.6$ μm at 5 Torr pressure. This entitles to expect faster and higher quality (debris-free, better morphology) hole drilling at low pressure and was observed experimentally for silicon.[14] Conditions of irradiation were kept similar to those in air albeit the difference in focusing: fluence was 70 J/cm^2 and irradiance was 4×10^{14} W/cm^2 for the focal spot diameter 9.5 μm and the depth of focus 212 μm.

Figure 4 shows SEM images of the rectangular holes cut in cover glass. Almost no debris were observed on front and rear surfaces, except a few larger spall-caused particles. Closer examination of the cut walls [Figs. 4(b) and 4(c)] showed no cracks on a micron-scale, which are usually observed in ps–ns pulse ablation of similar profiles.

On the rear surface a distinctive pattern of damage appeared around the rectangular holes as shown in Fig. 5(a). The width of the damage was $w=117$ μm for a 156-μm-thick cover glass plate. In order to determine the origin of the rear side damage we carried out several scans on the front side (without cutting through the sample) and examined the rear surface [Fig. 5(b)]. A pair of damage lines had appeared on the opposite side of the sample. Two scans were approximately reaching a 20–30 μm depth on the front surface. If scanning progressed more than two scans, the cut had deepened and, on the rear surface, the pair of damage lines was following on the rear side and moved towards center (the projection of the scanning line on the rear surface) as can be seen in Fig. 5. The same phenomenon took place in the case of quartz cutting in air as can be seen in Figs. 1 and 2. The mechanism of this phenomenon, most probably, can be explained by the stress wave propagation as discussed in Sec. 4.2.

Roughness of the cut walls are of great importance from application point of view. In Fig. 6, SEM image of the wall is shown with increasing resolution [(a)–(c)]. The ablation profile was produced by the elliptical concentric scan towards the center of structure. The wall had a distinct ripple-like pattern with period of 150–200 nm. Recently, similar structures were recognized from diffraction on embedded patterns recorded inside silica by fs pulses.[15]

For the same pulse energy density and scanning speed, we found that the volumetric ablation rate was approximately 3.5 times higher at 5 Torr pressure as compared with that in air. For a ten pulse ablation the volume removal was approximately 0.7 μm^3/μJ in air, while at 5 Torr it amounted to 2.5. This is a significant increase in the ablation rate, which was not observed in the case of hole drilling in steel.[16] For steel, where absorption is confined to the

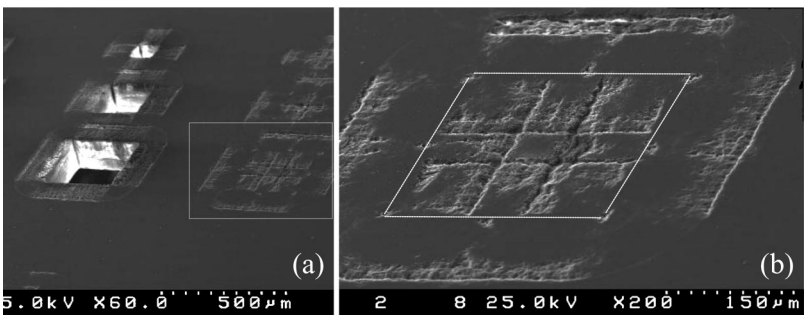

Fig. 5 SEM images of the rear side of glass sample shown in Fig. 4. (b) A close-up view of regions marked in (a) after two scans. Lines (b) show the perimeter of laser scans on the front surface. Irradiation conditions are specified in Fig. 4.

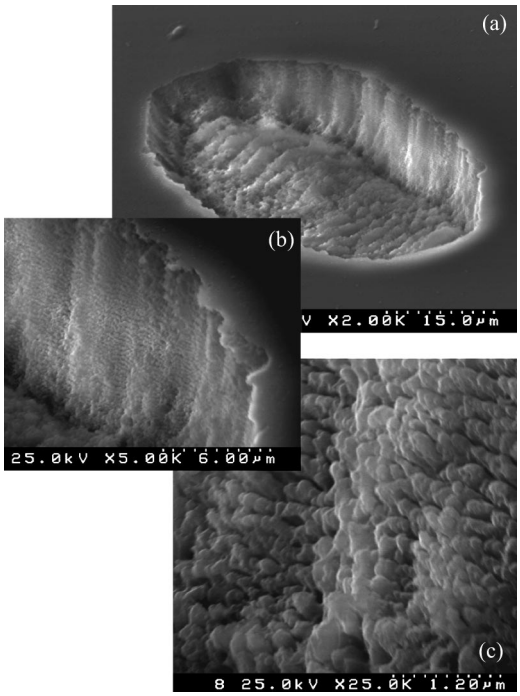

Fig. 6 Close-up SEM views of the elliptical ablation pattern produced after four consecutive concentric scans by pulses of 0.72 μJ energy focused by the objective lens of numerical aperture NA $=0.55$.

skin depth, the ablated volume was exactly the same for the air and 0.7 Torr pressure. The higher ablation speed at low pressure observed in the case of cover glass cutting could be explained by excitation of larger pre-surface volume as compared with the skin depth.

4 Discussion

4.1 *Mechanism of Laser Cut by Ablation*

First, let us evaluate fabrication conditions for an in-air cutting by fs-pulses focused onto a 21 μm spot with the long depth of focus $\simeq 2$ mm. Plasma spark was observed due to the dielectric breakdown at the pre-surface region of quartz sample. For example, for a pulse energy of $E_p = 200$ μJ the intensity would correspond to $I_p = 3.85 \times 10^{14}$ W/cm^2 at the employed focusing conditions. This is much larger than the intrinsic in-bulk dielectric breakdown of the known dielectrics, particularly glasses,[10,13] by more than one order of magnitude [e.g., the intrinsic breakdown threshold of BK7 (Schott) glass is 8.8×10^{12} W/cm^2 and it does not depend on pulse duration as it was demonstrated[17] for 0.4–30 ns pulses]. For a fused silica, a material very similar to quartz, the intrinsic in-bulk threshold of dielectric breakdown we had determined by additional experiment using microscope. Tight focusing by a high numerical aperture objective lens NA $=1.35$ at 10 μm depth was implemented to avoid aberrations and self-focusing.[18] At these conditions a *direct laser writing*[6] can be achieved and the intrinsic threshold of dielectric breakdown can be determined. The pulse energy at the focus was directly measured by using solid immersion lens (SIL) according to the procedure reported recently.[19] Pulse energy was found 12 nJ at the intrinsic breakdown at $\lambda = 800$ nm wavelength. Pulse duration at the focus was measured by GRENOUILLE technique[20] (Swamp Optics) using SIL. This technique allows us to record $time \times spectrum$ image of the pulse, and then, the pulse duration at full width at half maximum was retrieved by the frequency-resolved optical gating algorithm (Femtosecond technologies). The back propagation code (Swamp Optics) allowed us to exactly recalculate pulse duration at the point of interest. We found pulse duration of 175 ± 10 fs at focus, versus 140 fs at the output of a laser setup. Area of focus was calculated as the diameter of diffraction limited spot size $1.22\lambda/\mathrm{NA}$. Then, intensity per pulse at the intrinsic breakdown of fused silica was $I_p = 1.67 \times 10^{13}$ W/cm^2.

When translated, the ablation plasma spark made a line of the approximately 120 μm wide ($2w_0 \simeq 21$ μm) in a very first scan while subsequent scans were increasing the depth of the groove. The considerably wider cut line as compared with the beam waist is caused by an air breakdown at the pre-surface region. This unavoidable consequence of microstructuring by ablation in air as was demonstrated in the case of steel drilling.[16] Pulse energy, repetition rate, beam scanning speed must be optimized by taking into account the sample's thickness and material properties (primarily, a thermal conductivity), to maximize the ablation rate as shown in Fig. 3. This kind of fabrication inherently involves large volume removal by ablation, which helps to release a high temperature induced stress and prevent from cracking.

One of the advantages in cutting, scribing, and drilling of transparent materials by fs pulses of high intensity is the avoidance of plasma screening, which, in turn, allow to confine the HAZ. In the case of ablation by ultra-short pulses, electrons at the surface of sample can acquire kinetic energy in excess of the work function for a given material directly from the light field [see, e.g., Eq. (2)] or by inverse bremsstrahlung (a free-carrier absorption) and can escape from the surface of material. This drives a Coulomb explosion or disintegration of the surface by removal of surface ions in the high intensity electrical field, which has been build up due to the departing electrons.[21] This causes the ablation. Joule heating is less present as compared with the long-pulse (ns–ps) ablation, where the runaway process of material involves melting, boiling and phase explosion.

The quiver energy of an electron oscillating in a light field is given by[22]

$$\Omega(t) = \frac{e^2 E(t)^2}{4m\omega^2}, \tag{1}$$

where ω is the cyclic frequency of light, $E(t)$ is the time dependent strength of electric field of light, e, m are the electron charge and mass, respectively. In scaling form it reads[21]

$$\Omega[\mathrm{eV}] = 9.3(1+\epsilon^2)\frac{I}{10^{14}[\mathrm{W/cm^2}]}(\lambda[\mu\mathrm{m}])^2, \tag{2}$$

where $\epsilon = 1$ for the circular polarization and $\epsilon = 0$ for the linear. As one can evaluate from Eq. (2), the pulse intensity

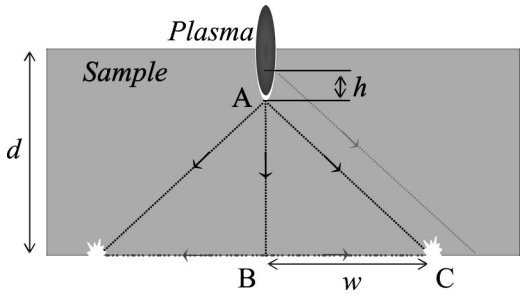

Fig. 7 Geometry of the stress waves generation. Thickness of sample was $d=156$ μm, the distance at which the damage appeared $w=117$ μm (measured from Fig. 5). Velocities of dilatation (compression), distortion, and surface Rayleigh waves are $c_l=5.80$, $c_t=3.35$, $c_R=3.08$ μm/ns (see Ref. 24), respectively.

of 10^{14} W/cm^2 corresponds to electron quiver energy of 6 eV for linear polarization (12 eV for the circular) at $\lambda=0.8$ μm. This energy acquired by an electron from the light field is comparable with the band gap of the most of glasses and quartz 8–10 eV and coincides with the onset of glass matrix absorption at approximately 210 nm. In this way, high intensity facilitates an almost instantaneous (within an optical cycle) ionization of the exposed material.

Let us compare conditions of our fabrication with predictions of Keldysh theory of multi-photon ionization. According to the theory,[23] the distinction between the dominance of multi-photon ionization (MPI) and tunneling in creation of free electrons depends on parameter γ in such a way that for $\gamma \gg 1$ MPI dominates while for $\gamma \ll 1$ the tunneling is the main mechanism providing free electrons. This parameter is given by[23]

$$\gamma = \frac{\sqrt{2mJ}\omega}{eE_0}, \quad \text{with} \quad E_0 = \sqrt{\frac{2I}{c\varepsilon_0 n}}, \tag{3}$$

where ω is the laser frequency, m and e are the mass and charge of the electron, $n=1.5$ is the refractive index of the material, I is the laser intensity at the focus, E_0 is the corresponding strength of electric field of light, and ε_0 is the permittivity of vacuum. The ionization potential J is taken equal to the typical band gap energy of glass $E_g=8$ eV [validity of Eq. (3) depends on fulfillment of condition $J/(\hbar\omega)>1$]. Then for $I=4\times10^{14}$ W/cm^2 one could find $\gamma=0.5$ from Eq. (3). Hence, the mechanism of free electron generation in our experiments was the mixture of multiphoton ionization and tunneling. Intensity of light at which an atom becomes unstable during period of light oscillation $2\pi/\omega$ can be evaluated as[23] $I_t=(\hbar\omega/J)^2 I_{\text{at}}$, where $I_{\text{at}} \simeq 10^{16}$ W/cm^2 is the light intensity corresponding to the Coulomb field of nucleus at first Bohr orbit in hydrogen atom. In our experiment I_t was 3.7% of I_{at} at $I=4\times10^{14}$ W/cm^2.

4.2 *Phenomenon of Rear Surface Damaging by Stress Waves*

In this section we explain the rear surface damage resulted from laser cutting in air and vacuum (Figs. 1 and 5). Figure 7 shows the relevant geometry. We found experimentally that $\widehat{\text{BAC}} \simeq 37°$ for a cover glass sample and this angle was independent on the thickness d of the sample, i.e., $w/d=\text{Const}$. The rear side damage appeared after approximately two scans, which had produced the 10–30 μm deep grooves (dependent on pulse energy) on the front surface. Further scans had deepened the cut line while the damage of the rear side was closing on the point B (Fig. 7) from the both sides simultaneously as can be seen in SEM images (Fig. 5). Also, one can see form Fig. 5(b) that the center of the backside pattern is damaged more extensively than the outer lines. A spall-like morphology of the rear damage suggested that the stress waves generated by the plasma ablation plume might be responsible for this phenomenon. Other effects, such as white light generation, self-focusing, refraction on the bottom of the cut line, and diffraction on the ripple-like walls of the cut were excluded upon closer inspection of geometrical details.

Let us consider the stress generation at point A (Fig. 7) by a plume pressure pulse. The longitudinal dilatation (compression) wave travels in isotropic media fastest at velocity $c_l \simeq 5.8$ km/s (5.8 μm/ns) in glass.[24] Simultaneously launched transverse (distortional) waves travel in glass by a factor $\sqrt{3}$ slower, $c_t=c_l/\sqrt{3}$. The ratio c_l/c_t is determined by the elastic constants of media. Propagation of both waves are radial. At the surface, the Rayleigh surface wave can be excited upon the incidence of the transverse waves. Velocity of this type of wave is lower than the c_t by a factor κ, which solely depends on the Poisson ratio, ν[24]:

$$\kappa^6 - 8\kappa^4 + (24 - 16\alpha^2)\kappa^2 + 16\alpha^2 - 16 = 0, \tag{4}$$

where $\alpha=\sqrt{(1-2\nu)/(2-2\nu)}$ and for a glass $\kappa=0.9$ (the value $\nu=0.17$ of silica glass was used for evaluation).[24] Here, the only solution of Eq. (4) which satisfies $c_R<c_t$ should be considered as it was determined in the original work of Rayleigh.[24] With these velocities determined and dimensions d and w directly measured one can find, that there is no possibility for two stress waves to collide at point C (Fig. 7) if the waves are launched at point A simultaneously, i.e., in volume the stress (both, the dilatation and distortion) travels too fast to meet the Rayleigh wave at point C where the damage was observed experimentally.

Collision of which two waves is causing the rear surface damage? The surface Rayleigh and compression waves could collide at C only if the surface wave was launched by approximately 30 ns before the dilatation one. This value is very close to the 26 ns necessary for a distortion wave to travel distance AB (only the distortion wave can excite the surface Rayleigh wave). The other option is a collision of surface and distortion wave, however, the expected distance w should be approximately 330 μm in such case. Hence, the former mechanism took, most likely, place in our experiments. Actually, the pressure load by a plasma plume at point A lasts about 100 ns after fs-pulse hit the surface[16] and this can explain the necessary time delay for the two wave collision.

An appropriate scenario of collision of two stress waves on a rear surface could be following. The Rayleigh wave was excited by the transverse distortion wave, which arrived from the early stages of the ablation pressure pulse,

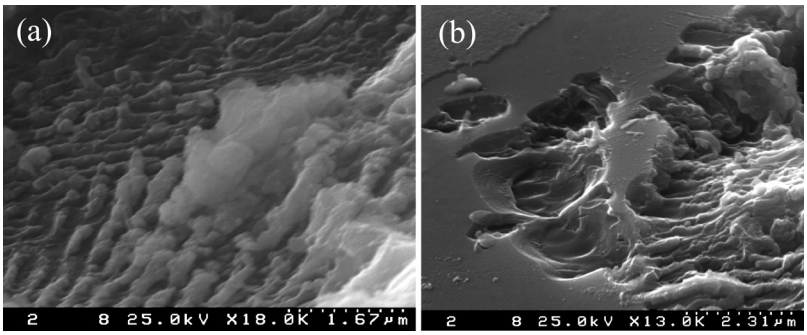

Fig. 8 SEM images of the rear-side damage morphology: (a) from the region near the point *C* (Fig. 7) and (b) from location in the middle of *BC*.

while the dilatation wave, launched approximately 30 ns later at the maximum of the ablation pressure, was responsible for a resulting stress, which broke the elasticity limit of glass and caused spalling. Energy carried by stress waves in the half-infinite medium is distributed as 67%, 26%, and 7% for the Rayleigh, distortion, and dilatation waves, respectively.[25] The waves' amplitude perpendicular to the surface scales similarly. For the proposed scenario to be valid, the duration of pressure pulse should be at least 60 ns. This duration of the plume pulse fit well the reported observations.[16] The time difference in launching Rayleigh and dilatation waves may also be caused by the difference in location where the corresponding waves starts (this is schematically shown by the height difference, h, in Fig. 7). The relevance of stress waves to the rear surface damage is, also, corroborated by observation of back-side edges of the cut-through lines. Usually, the rims had spall features at elevated pulse energies. This is a direct consequence of the reflection of the dilatation (compression) and distortion (shear) waves from the rear surface. At reflection a tension stress is formed;[24] if large enough, it could break through the remaining thin part of the bottom wall causing the spall.

Morphology of the rear-side damage at point *C* (Fig. 7) showed a periodic structures of 50–400 nm (Fig. 8). This is an interesting result of self-organization of the surface after spalling. It appears that a stress-induced spalling took place at elevated temperatures (over the glass transition temperature $T_g > 600°C$ for a borosilicate cover glass), which caused melting observable in some of the damage sites [Fig. 8(b)].

We can conclude that the stress waves play an important role in fs-laser fabrication, which is sometimes erroneously considered ''non-thermal.'' This phenomenon of the rear-side surface damage is expected to occur in non-transparent brittle materials as well.

5 Conclusions

Cutting of quartz and glass by 150 fs, 800 nm wavelength pulses (in spectral region of high transmission) at 1 kHz repetition rate using a simple lens focusing is demonstrated at the ambient and 5 Torr air pressure. When the length of focus is comparable or longer than the thickness of sample, a cracking and debris free cutting was achieved by optimizing pulse energy, scanning speed, and ambient pressure. Thickness of the cutting line varies from 30 to 150 μm and depends on the focusing conditions and pulse energy. At a low 5 Torr air pressure the volumetric ablation rate was 3.5 times enhanced as compared with the in-air ablation. The stress waves-induced fracture of the rear surface of glass samples was observed. This phenomenon might prove be useful for a surface microstructuring.

Acknowledgments

This work was partially supported by the U.S.A. Aerospace R&D Contract No. F62562-03-P-0208 AOARD 02-35. The authors also acknowledge fruitful discussions with Dr. O. M. Efimov and Dr. A. V. Rode.

References

1. K. M. Davis, K. Miura, N. Sugimoto, and K. Hirao, *Opt. Lett.* **21**, 1729–1731 (1996).
2. C. B. Schaffer, A. Brodeur, J. F. García, and E. Mazur, *Opt. Lett.* **26**(2), 93–95 (2001).
3. H. Misawa, Jpn. patent application No. 023614 (1995).
4. M. Watanabe, H.-B. Sun, S. Juodkazis, T. Takahashi, S. Matsuo, Y. Suzuki, J. Nishii, and H. Misawa, *Jpn. J. Appl. Phys., Part 2* **27**(12B), L1527–L1530 (1998).
5. H. Sun, Y. Xu, S. Juodkazis, K. Sun, M. Watanabe, S. Matsuo, H. Misawa, and J. Nishii, *Opt. Lett.* **26**(6), 325–327 (2001).
6. M. Miwa, S. Juodkazis, T. Kawakami, S. Matsuo, and H. Misawa, *Appl. Phys. A: Mater. Sci. Process.* **73**(5), 561–566 (2001).
7. H. Sun, V. Mizeikis, S. Juodkazis, J.-Y. Ye, S. Matsuo, and H. Misawa, *Appl. Phys. Lett.* **79**(1), 1–3 (2001).
8. M. Watanabe, Thesis, Tokushima Univ., Japan (BSc 1996, MSc 1998).
9. A. Marcinkevicius, S. Juodkazis, M. Watanabe, M. Miwa, S. Matsuo, H. Misawa, and J. Nishii, *Opt. Lett.* **26**(5), 277–279 (2001).
10. S. Juodkazis, A. V. Rode, E. G. Gamaly, S. Matsuo, and H. Misawa, *Appl. Phys. B: Lasers Opt.* **77**, 361–366 (2003).
11. K. Yamasaki, S. Juodkazis, S. Matsuo, and H. Misawa, *Appl. Phys. A: Mater. Sci. Process.* **77**, 371–373 (2003).
12. A. E. Siegman, *Lasers*, University Science, Mill Valley, CA (1986).
13. E. Vanagas, I. Kudryashov, D. Tuzhilin, S. Juodkazis, S. Matsuo, and H. Misawa, *Appl. Phys. Lett.* **82**(17), 2901–2903 (2003).
14. V. Mizeikis, S. Juodkazis, J.-Y. Ye, A. V. Rode, S. Matsuo, and H. Misawa, *Thin Solid Films* **438–439**, 445–451 (2003).
15. J. D. Mills, P. G. Kazansky, and E. Bricchi, *Appl. Phys. Lett.* **81**(2), 196–198 (2002).
16. F. Dausinger, H. Hügel, and V. Konov, *SPIE Proc*, **5147**, 106–115 (2003).
17. O. M. Efimov, V. S. Popikov, and M. J. Soileau, *J. Opt. Technol.* **63**, 120–125 (1996).
18. A. Marcinkevicius, V. Mizeikis, S. Juodkazis, S. Matsuo, and H. Misawa, *Appl. Phys. A: Mater. Sci. Process.* **76**, 257–260 (2003).
19. S. Matsuo and H. Misawa, *Rev. Sci. Instrum.* **73**, 2001–2013 (2002).
20. P. O'Shea, M. Kimmel, X. Gu, and R. Trebino, *Opt. Lett.* **26**(12), 932–934 (2001).
21. E. G. Gamaly, A. V. Rode, V. T. Tikhonchuk, and B. Luther-Davies, *Phys. Plasmas* **9**(3), 949–957 (2002).
22. E. Yablonovitch, *Phys. Rev. Lett.* **60**(9), 795–796 (1988).
23. N. I. Koroteev and I. L. Shumai, *Physics of Intense Laser Radiation*, Nauka, Moscow (1991).
24. H. Kolsky, *Stress Waves in Solids*, Dover Phoenix Editions, Mineola, NY (2003).
25. K. F. Graff, *Wave Motion in Elastic Solids*, Dover, New York (1975).